Research
A SCIENCE PARTNER JOURNAL

RESEARCH ARTICLE

Laser-Induced Methanol Decomposition for Ultrafast Hydrogen Production

Weiwei Cao[1,2†], Yinwu Li[2†], Bo Yan[1,2†], Zhiping Zeng[1,2], Pu Liu[1,2], Zhuofeng Ke[2*], and Guowei Yang[1,2*]

[1]State Key Laboratory of Optoelectronic Materials and Technologies, Nanotechnology Research Center, Sun Yat-sen University, Guangzhou 510275, P. R. China. [2]School of Materials Science and Engineering, Sun Yat-sen University, Guangzhou 510275, P. R. China.

*Address correspondence to: kezhf3@mail.sysu.edu.cn (Z.K.); stsygw@mail.sysu.edu.cn (G.Y.)
†These authors contributed equally to this work.

Citation: Cao W, Li Y, Yan B, Zeng Z, Liu P, Ke Z, Yang G. Laser-Induced Methanol Decomposition for Ultrafast Hydrogen Production. *Research* 2023;6:Article 0132. https://doi.org/10.34133/research.0132

Submitted 24 February 2023
Accepted 11 April 2023
Published 9 May 2023

Copyright © 2023 Weiwei Cao et al. Exclusive licensee Science and Technology Review Publishing House. No claim to original U.S. Government Works. Distributed under a Creative Commons Attribution License (CC BY 4.0).

Methanol (CH_3OH) is a liquid hydrogen (H_2) source that effectively releases H_2 and is convenient for transportation. Traditional thermocatalytic CH_3OH reforming reaction is used to produce H_2, but this process needs to undergo high reaction temperature (e.g., 200 °C) along with a catalyst and a large amount of carbon dioxide (CO_2) emission. Although photocatalysis and photothermal catalysis under mild conditions are proposed to replace the traditional thermal catalysis to produce H_2 from CH_3OH, they still inevitably produce CO_2 emissions that are detrimental to carbon neutrality. Here, we, for the first time, report an ultrafast and highly selective production of H_2 without any catalysts and no CO_2 emission from CH_3OH by laser bubbling in liquid (LBL) at room temperature and atmospheric pressure. We demonstrate that a super high H_2 yield rate of 33.41 mmol·h^{-1} with 94.26% selectivity is achieved upon the laser-driven process. This yield is 3 orders of magnitude higher than the best value reported for photocatalytic and photothermal catalytic H_2 production from CH_3OH to date. The energy conversion efficiency of laser light to H_2 and CO can be up to 8.5%. We also establish that the far from thermodynamic equilibrium state with high temperature inside the laser-induced bubble and the kinetic process of rapid quenching of bubbles play crucial roles in H_2 production upon LBL. Thermodynamically, the high temperature induced using laser in bubbles ensures fast and efficient release of H_2 from CH_3OH decomposition. Kinetically, rapidly quenching of laser-induced bubbles can inhibit reverse reaction and can keep the products in the initial stage, which guarantees high selectivity. This study presents a laser-driven ultrafast and highly selective production of H_2 from CH_3OH under normal conditions beyond catalytic chemistry.

Introduction

Hydrogen (H_2) energy, the cleanest energy source with a high energy density, is one of the foundations of the future energy system [1–3]. However, H_2 is flammable and explosive, as well as inconvenient for transport [4,5]. Therefore, in situ H_2 production is an effective way to solve this problem. Methanol (CH_3OH) is a promising liquid H_2 carrier and is widely used for H_2 production [6,7]. Thermocatalytic CH_3OH reforming is a traditional technique of releasing H_2 from CH_3OH, but this process needs to be carried out at relatively high temperatures (usually 200 °C) and, at the same time, a large amount of carbon dioxide (CO_2) is emitted [8–12]. Therefore, scientists have been looking for mild and sustainable ways to produce H_2 from CH_3OH. Photocatalysis and photothermal catalysis carried out at a normal temperature have attracted extensive attention [12–16]. However, for these methods above, to avoid carbon monoxide (CO) poisoning of a catalyst, CO_2 emission is inevitable [17–19]. This should be detrimental to carbon neutrality and exacerbate a greenhouse effect. In fact, CO can be used as fuel [20]. Thus, how to realize the efficient and rapid release of H_2 from CH_3OH without CO_2 emission under mild conditions is indeed a challenge.

Here, we, for the first time, report an ultrafast and highly selective production of H_2 without any catalysts and no CO_2 emission from CH_3OH by laser bubbling in liquid (LBL) at a normal temperature and pressure. LBL means that the pulsed laser is focused below the liquid level to produce small bubbles in liquid as shown in Fig. 1. Note that the temperature inside the laser-induced bubble can reach as high as about 10^4 K [21,22]. At such high temperatures, the ionization temperature of CH_3OH has been exceeded, thus generating CH_3, CH_3O, and CH_2OH radicals as well as CH_3O^-, OH^-, and H^+ ions in the bubble. At the same time, these bubbles would quench at a very short time because of the confining and cooling effect of the surrounding liquid, which would cause that the primary products of high-temperature chemical reactions occurring inside bubbles are directly frozen and retained at room temperature [23–25]. Our measurements show that, in such a local extreme environment inside bubbles, CH_3OH is directly to release H_2 (33.41 mmol·h^{-1}) and CO (16.88 mmol·h^{-1}). The production rate of H_2 is much higher than that of photocatalytic

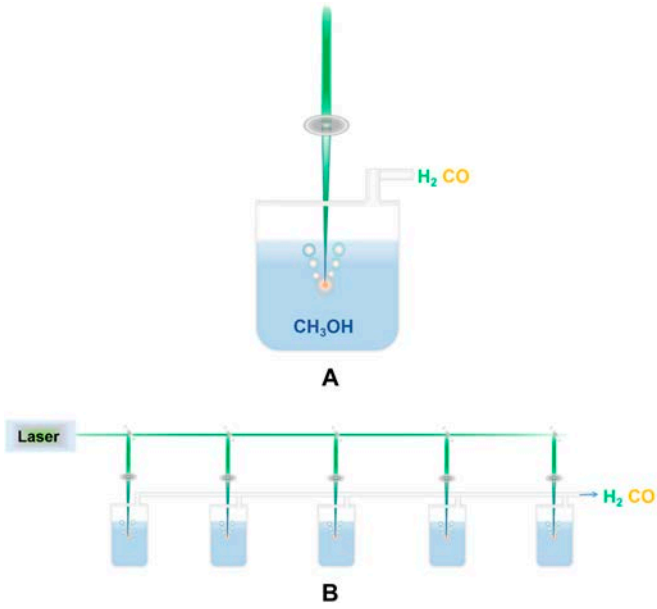


Fig. 1. Schematic illustration of the experiment set. (A) A second harmonic is produced using a Q-switched Nd:YAG laser with a pulse wavelength of 532 nm and a pulse width of 10 ns. A pulsed laser is focused inside the liquid, forming a spot size of about 1 mm. Finally, the gas produced by the reaction is collected. (B) A laser-driven amplification scheme of H_2 release from CH_3OH is proposed, which divides the beam into multiple beams of light, forms an array, and expands the scale of production.

and photothermal catalysis. Meanwhile, the selectivities for H_2 and CO are up to 94.26% and 89.25%, respectively. At 700 mJ per pulse of laser energy, the conversion efficiency from laser light to H_2 and CO can reach 8.5%. Notably, there is no CO_2 emission. Additionally, we establish the mechanism of laser-driven CH_3OH releasing H_2, including the thermodynamics and kinetics of high-temperature reactions in the bubble upon the LBL process. In terms of thermodynamics, the extreme high temperature of the bubble caused using laser promotes the efficient reaction and ensures a high yield. From a kinetic point of view, the rapid quenching process of bubbles freezes the final product, and the high-energy barrier of the reverse reaction prevents the product from returning to CH_3OH. Therefore, the synergistic effect of thermodynamics and kinetics ensures the high yield and selectivity of H_2 release from CH_3OH. Therefore, these results show that the laser-driven direct decomposition of CH_3OH to release H_2 has great potential in the industry.

Results and Discussion

A schematic of the experimental setup is shown in Fig. 1, and the whole LBL process was carried out at room temperature and atmospheric pressure. In this case, LBL is used to enable rapidly switching reactions between high temperature and room temperature to achieve the release of H_2 from CH_3OH (Fig. 1A). When LBL is performed, the bubbles are generated instantaneously using the focused laser and then collapsed in several hundred microseconds. A series of high-temperature chemical reactions would occur before the collapse of bubbles, and then products would be released together with the collapse of bubbles. Note that after the experiment was completed, the solution temperature remained basically unchanged. Figure 1B shows our proposal for the laser-driven H_2 production from CH_3OH in practical applications. When the laser energy is excess, the laser beam can be divided to make the energy utilization rate higher. Dividing laser into multiple reaction devices to assemble them into an array can enhance the production rate for large-scale operations. Evidently, this technique opens a new direction for the industrial realization of H_2 production from CH_3OH.

A series of measurements of the samples were performed as shown in Fig. 2. The yields of the generated gases positively correlated with the laser energy (Fig. 2A). The H_2 yield is close to 0 when the laser energy is below 100 mJ per pulse and then increases with the increase of laser energy. Therefore, the 100 mJ per pulse is the threshold of laser energy for the reaction to occur. When the laser energy is higher than 100 mJ per pulse, the reaction can be carried out and a large amount of H_2 can be produced. At 700 mJ per pulse, the yields of H_2 and CO can reach 33.41 and 16.88 $mmol \cdot h^{-1}$, respectively. These results can be attributed to the increase in the temperature in bubbles caused by the increase in the laser energy, which leads to more efficient high-temperature chemical reactions. It is worth noting that the process has only trace amounts of CH_4, C_2H_4, C_2H_6, and C_2H_2 generation, which have rates that were only 0.56, 0.22, 0.073, and 1.18 $mmol \cdot h^{-1}$ (Fig. S1), respectively. More importantly, there is no CO_2 generation in the LBL process. In addition to adjusting the laser energy, we study the frequency effect of the pulsed laser. As can be seen from Fig. 2B, the maximum yield (33.41 $mmol \cdot h^{-1}$) of H_2 was reached at the frequency of 10 Hz. However, only 3.34 $mmol \cdot h^{-1}$ of H_2 and 1.76 $mmol \cdot h^{-1}$ of CO were measured at 1 Hz. Therefore, this result can be attributed to more bubble generation per unit of time with an increase in the frequency of pulsed laser. To investigate the effect of the reaction time on the yield rate, gas samples at various reaction times at 700 mJ per pulse of laser energy were collected to calculate the yield rate. As shown in Fig. 2C, the laser action time had no obvious effect on the yield rate at the same laser energy. This is mainly because the gas product is released as the bubble collapses, then the surrounding CH_3OH solution will replenish this reaction area, and new bubbles will be generated again. Importantly, the laser-driven CH_3OH decomposition releases H_2 and CO with a high selectivity, up to 94.26% and 89.25%, respectively, as shown in Fig. 2D. Therefore, these results show that H_2 yield does not change with laser action time and further elucidate that this method can sustainably release H_2 from CH_3OH over a long period of time through a laser-driven process. In addition, we also study the energy conversion efficiency from laser light to H_2 and CO. Figure 2E shows that, with the increase of laser energy, the conversion efficiency is also higher, and the energy conversion efficiency can be as high as 8.5% at 700 mJ.

To evaluate advanced performance of LBL, we compared H_2 yield rates of LBL with that of photocatalytic and photothermal catalytic H_2 release from CH_3OH as shown in Table. Considering the characteristic terms involved in photocatalytic and photothermal catalytic CH_3OH releasing H_2, such as solution and irradiation area, the yield rate was normalized into 1-mm space dimensions (e.g., irradiation area and the laser-focused spot). From Table, we can clearly see that the laser-driven H_2 production from CH_3OH is 3 orders of magnitude higher than the best value of photocatalysis and photothermal catalysis to date.

Accordingly, these experimental results above suggest that CH_3OH can efficiently release a large amount of H_2 and CO upon the LBL process, and the yield rate can be flexibly regulated by changing the energy and frequency of the pulsed laser.

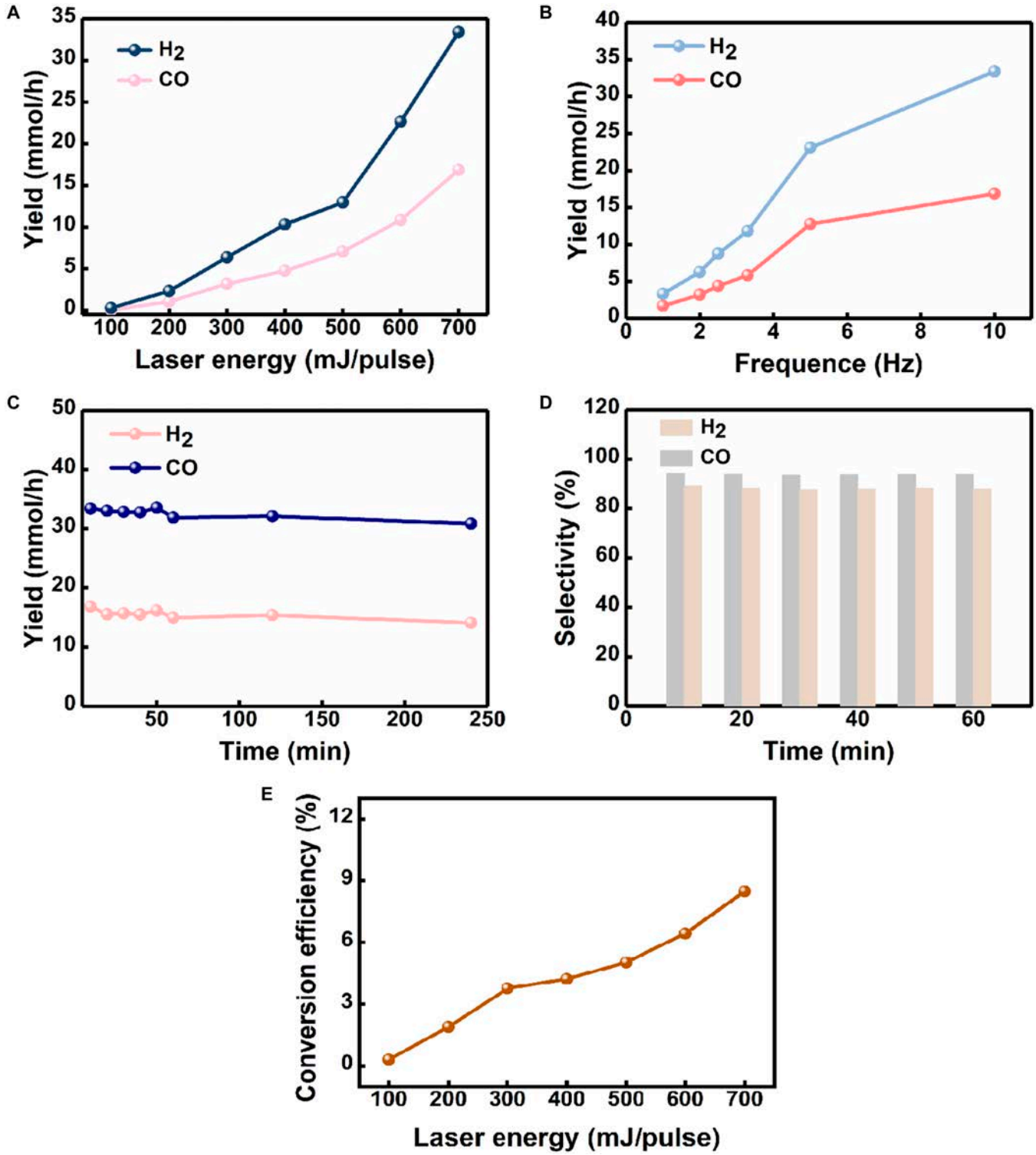


Fig. 2. Measurement and characterization of the products. (A)The yield rate versus laser energy and (B) frequency of pulsed laser. (C) The yield rate and (D) selectivity of H_2/CO at different times under 700 mJ per pulse of laser energy. (E) Laser-to-hydrogen conversion efficiency versus laser energy.

Additionally, ultrafast and highly selective production of H_2 and CO without CO_2 emission from CH_3OH can be achieved by LBL.

To have a deep understanding to CH_3OH decomposition reaction under the LBL process, the theoretical research was taken on the basis of the density functional theory (DFT) calculation, aiming to explain the high-temperature chemical reactions occurring inside bubbles upon the LBL process. The pulsed laser would lead to the high-temperature environment, which promotes the CH_3OH decomposition reaction. As shown in Fig. 3A, the 3 possible reaction paths are the (a) ion path, (b) radical path, and (c) direct decomposition path, respectively. In the ion paths, CH_3OH can be decomposed into a series of ions species: CH_3O^-/H^+ (165.2 kcal/mol), CH_2OH^-/H^+

Table. Comparison of laser-driven H_2 release from CH_3OH with photocatalytic and photothermal catalytic H_2 release from CH_3OH at ambient temperature and pressure.

Normalized yield ($mmol \cdot h^{-1}$)	H_2 production rate	Characteristic terms (irradiation area, catalyst loading, solution)	Reference
9.1×10^{-4}	14 $mmol \cdot h^{-1} \cdot g^{-1}$ cat	3.84 cm^2, 25 mg, MeOH/H_2O (v/v = 1/1)	Cui et al. [25]
2.9×10^{-2}	328 $mmol \cdot h^{-1} \cdot g^{-1}$ cat	8.5-mm diameter, 5 mg, CH_3OH/H_2O (v/v = 1/4)	Luo et al. [13]
6.6×10^{-2}	310 $mmol \cdot h^{-1} \cdot g^{-1}$ cat	0.0471 m^2, 10 g, CH_3OH/H_2O (v/v = 1/1.6)	Li et al. [12]
3.34×10^{1}	33.4 $mmol \cdot h^{-1}$	1-mm diameter, catalyst-free, CH_3OH	This study

(166.0 kcal/mol), and CH_3^+/OH^- (−16.2 kcal/mol). The ions species are located at high-activation free energy, which are less favorable for the CH_3OH decomposition, while the radical paths are more favorable for the CH_3OH decomposition. As shown in Fig. S3, the formation of radical species requires lower temperature than that of ion species. When the reaction temperature is high than about 4,000 K, the $CH_3OH^{\bullet}/H^{\bullet}$ and $CH_2OH^{\bullet}/H^{\bullet}$ can form. The radical species $CH_3O^{\bullet}/H^{\bullet}$ (−172.5 kcal/mol), $CH_2OH^{\bullet}/H^{\bullet}$ (−184.2 kcal/mol), and $CH_3^{\bullet}/OH^{\bullet}$ (−244.0 kcal/mol) are located at low-activation free energy. By releasing H_2, both of $CH_3O^{\bullet}/H^{\bullet}$ and $CH_2OH^{\bullet}/H^{\bullet}$ species can form the key intermediate CH_2O (−254.0 kcal/mol). The CH_2O can be further decomposed via radical intermediate $CHO^{\bullet}/H^{\bullet}$ (−400.3 kcal/mol), resulting in the final product CO and H_2 (−500.9 kcal/mol). In addition, the formation of C_2H_6, C_2H_4, C_2H_2, and CH_4 are shown in Fig. S4, which are initial from the key radical species $CH_3^{\bullet}/OH^{\bullet}$. The coupling of 2 $CH_3^{\bullet}$ species would result in C_2H_6, which can form the C_2H_4 and C_2H_2 by releasing H_2, while the coupling between $CH_3O^{\bullet}/H^{\bullet}$ and $CH_3^{\bullet}/OH^{\bullet}$ species would lead to CH_4 and CH_2O, which can generate CO by releasing H_2. Furthermore, the direct decomposition paths have been studied as well. However, the transition states for the direct decomposition paths are located at high-activation free energy: TS_1 (102.2 kcal/mol), TS_2 (−174.9 kcal/mol), and TS_3 (−155.5 kcal/mol).

Moreover, the ab initio molecular dynamics (MD) simulations were performed to explain the high-temperature chemical reaction of CH_3OH in bubbles. The simulation temperatures are 298, 5,000, and 10,000 K, respectively, aiming to explore the temperature effect of pulsed laser with different energies. As the temperature rises from 298 to 5,000 K, the H_2, CO, H_2O, CH_2O, and hydrocarbon products were observed in MD simulation (Fig. 3B and C). When the temperature rises to 10,000 K, a large amount of H_2 and CO products were generated (Fig. 3D). Furthermore, the distributions of radial distribution functions (RDFs) exhibited the decomposition of the CH_3OH. As the temperature rises to 10,000 K, the maximum distribution of hydrogen–hydrogen was shifted from 1.75 to 0.75 Å (Fig. 3E), while the maximum distribution of carbon–oxygen was changed from 1.45 to 1.25 Å (Fig. 3F). The hydrogen–hydrogen and carbon–oxygen RDFs show the formation of the H_2 and CO molecules. In addition, the carbon–carbon RDF further suggested the formation of ethylene and acetylene (Fig. S5).

To further understand the mechanism of laser-driven H_2 release from CH_3OH, we propose basic physical and chemical perspectives on the basis of the experimental measurements, DFT calculations, and MD simulations as shown in Fig. 4. First, when the pulsed laser is focused below the liquid level, many small bubbles form in the solution (Fig. 4A). A high-energy laser can induce high temperatures up to thousands of kelvin inside the bubble, and this extreme high temperature can exceed the ionization temperature of CH_3OH in the bubble, which results in the formation of CH_3, CH_3O, and CH_2OH radicals as well as CH_2OH^-, OH^-, and H^+ ions in the bubble (Fig. 4B). Note that the state in the bubble is far from thermodynamic equilibrium. Therefore, these laser-induced bubbles provide a favorable thermodynamic environment for the CH_3OH decomposition.

On the basis of Eyring's transition state theory, the temperature and the activation free energy are 2 key factors for the chemical reaction rate processes. By comparing with each reaction step in Fig. S6, the CH_3OH decomposition is an exothermic reaction in the whole process. The reduction of activation free energy is mainly due to the entropy increase of the reactions. As shown in Fig. S6, the ΔS are 27.8 and 24.7 cal/mol for the formation of CH_2O and CO reactions, respectively. In the LBL process, the bubble environment is located at the high temperature, which amplifies the entropy effect. Thus, these results show that the entropy effect plays an important role in the reaction process at a high temperature, which can directly and effectively promote the decomposition of CH_3OH to release H_2.

Kinetically, the pulsed laser results in an instantaneous formation of bubbles at the focal point inside of the CH_3OH solution. According to previous studies, far from equilibrium bubbles would disintegrate within 100 to 400 μs [21], enabling ultrafast H_2 release from CH_3OH. Because the temperature drops to room temperature instantaneously, during the rapid cooling process, H_2 and CO of the products formed by the high temperature can be retained, preventing the products from slowly decomposing and returning those to the initial state. Because of the rapid quenching of bubbles, the formation of free radical species is prevented. The activation free energy of the formation of $CH_2OH^{\bullet}/H^{\bullet}$ is 86.6 kcal/mol in 298.15 K. In addition, the CO and H_2 conversion reaction are carried out in 298.15 K as well (Fig. S7). The rate-determining step of CO conversion is the formation of CHOH, which undergoes the transition state TS_3-iso. The activation free energy of this step is 81.0 kcal/mol. The temperature for a practical CO and H_2 conversion reaction ($t_{1/2}$ = 1 s to 1 h) is around 866.3 to 1038.9 K (Fig. S8). The results clearly suggested that the CO and H_2 conversion are almost nonoccurrence below 1038.9 K. Additionally, the MD simulations were taken to simulate the rapid cooling stage of the LBL process. The RDFs results suggest that the H_2 and CO species are retained in high proportion (Figs. S9 and S10).

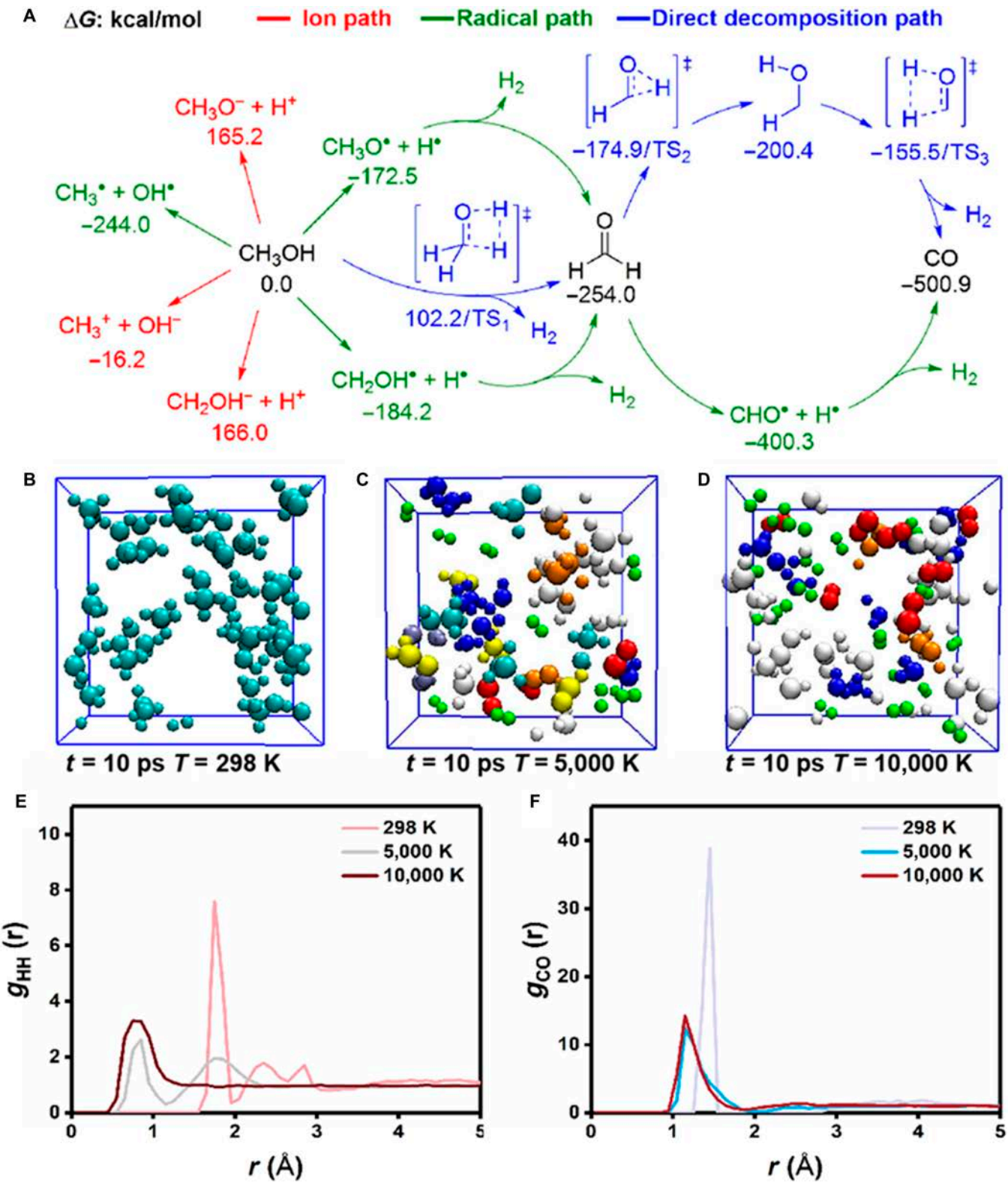


Fig. 3. Theoretical calculations and simulations for CH_3OH decomposition upon LBL. (A) Mechanism for CH_3OH decomposition under the LBL process. The free energies calculated in 10,000 K. (B to D) Configurations of the nonadiabatic ab initio MD simulations. H_2, CO, CH_3OH/CH_3O, H_2O, CH_2O, $CH_4/C_2H_4/C_2H_2$, and other intermediates are shown in green, red, cyan, blue, yellow, orange, and white colors, respectively. (E and F) H–H and C–O radial distribution functions. The radial distribution functions are calculated for 500 fs for each temperature.

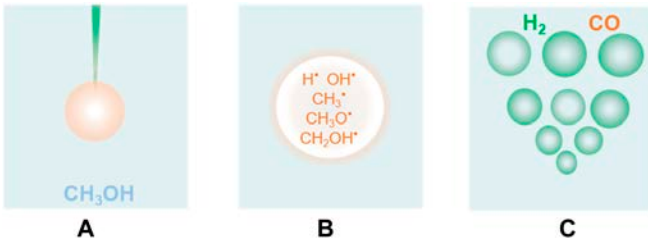


Fig. 4. Mechanism of laser-driven H_2 release from CH_3OH. (A) A pulsed laser is focused below the solution surface to trigger bubbles. (B) The laser-induced bubble contains some high-energy ions from CH_3OH, such as $CH_3^•$, $H^•$, and $CH_2OH^•$. The bubble is a miniature reactor. (C) The products are released along with bubbles' rapid collapsing.

When the bubble induced using laser expands to the maximum volume in CH_3OH, it is close to the vacuum state because the number of internal molecules does not change much. The external liquid pressure acts on the bubble, and the resulting pressure difference causes the bubble to collapse quickly. Therefore, rapid quenching of nonequilibrium ensures the formation of CO/H_2 products in laser-induced high-temperature chemical reactions in bubbles, as well as prevented the products from further reversion to initial states. As a result, large amounts of H_2 and CO are released as the bubble collapsed, and the process can achieve a high product yield (Fig. 4C).

Therefore, the LBL process can be carried out at room temperature and atmospheric pressure, which is simple and has no CO_2 emissions. The nonequilibrium process of bubbles is similar to the microreactor induced using a laser, in which the high-temperature chemical reaction takes place, which can proceed the reaction more effectively. Moreover, the extremely short quenching time can keep the product at room temperature and inhibit the reverse reaction.

Conclusion

In summary, we developed an ultrafast and highly selective production of H_2 and CO without a catalyst as well as no CO_2 emission from CH_3OH driven using laser under normal temperature and pressure. A super high H_2 yield rate of 33.41 mmol·h^{-1} with 94.26% selectivity can be produced upon the laser-driven process, and this yield is 3 orders of magnitude higher than the best value reported for photocatalytic and photothermal catalytic H_2 production from CH_3OH to date. On the basis of DFT calculation and MD simulation, we clarified the basic physical and chemical processes of laser-driven ultrafast H_2 release from CH_3OH, which confirm the experimental measurements of high temperature promoting CH_3OH decomposition. We also establish that the thermodynamic and kinetic mechanism of high-temperature chemical reactions inside bubbles induced pulsed laser. Thermodynamically, the high temperature of bubbles amplifies the entropy effect during the CH_3OH decomposition, which reduces the activation energy of the decomposition process without catalysts. Kinetically, the bubbles have a short quenching time, which makes it difficult for the products H_2 and CO to return to their initial states through a reverse reaction. Therefore, this synergy between thermodynamics and kinetics results in high yield and selectivity for H_2 and CO. Accordingly, we believe that LBL can be expected to be a disruptive technology to release H_2 from CH_3OH without CO_2 emission at normal conditions beyond catalytic chemistry.

Materials and Methods

Synthesis and characterization

First, CH_3OH (200 ml) was poured into a quartz reactor. Then, the second harmonics generated using a Q-switched Nd:YAG (neodymium-doped yttrium aluminum garnet crystal) laser device with a wavelength of 532 nm; a pulse width of 10 ns; repetition rates of 1, 5, and 10 Hz; and laser pulse energies of 100 to 700 mJ was focused inside the liquid, forming a spot size of about 1 mm. Moreover, not only the argon (Ar) gas is introduced into the solution, which can play the role of a protective gas, but also the gas produced during the reaction that flowed out together with the Ar. Before the experiment, the Ar gas was a bubble in CH_3OH (0.4 l/min) for 60 min to ensure that no air was present in the water. Gases produced by the laser-driven CH_3OH decomposition process were collected and characterized. The yields of gases (y_{CO}, y_{H2}, y_{C2H2}, y_{C2H4}, y_{CH4}, and y_{C2H6}) under diverse laser energy and time were quantified by gas chromatography (GC-2014C, Shimadzu) with a thermal conductivity detector (5Å molecular sieve column) and 2 flame ionization detectors (MC-3 column). The formula for calculating H_2 (S_{H2}) and CO (S_{CO}) product selectivity was as follows:

$$S_{CO} = \frac{y_{CO}}{y_{CO} + y_{C_2H_2} + y_{C_2H_4} + y_{CH_4} + y_{C_2H_6}} \times 100\%$$

$$S_{H_2} = \frac{y_{H_2}}{y_{H_2} + y_{C_2H_2} + y_{C_2H_4} + y_{CH_4} + y_{C_2H_6}} \times 100\%$$

Considering the enthalpy change of CH_3OH decomposing to H_2 and CO is as follows:

$$CH_3OH \longrightarrow CO + H_2,\ \Delta H = 128.07\ \text{kJ/mol}$$

The formula for calculating conversion of laser light to H_2 and CO product selectivity was as follows:

$$\eta\,(\%) = \frac{\Delta H \times n(\text{methanol})}{\text{laser energy}\,(\text{mJ/pulse}) \times 10\ \text{Hz} \times 3{,}600\ \text{s/h}} \times 100\%$$

where η is the energy conversion of laser light to H_2 and CO, ΔH is the enthalpy change from CH_3OH to CO and H_2, and n(methanol) is the amount of CH_3OH that takes part in reaction.

Calculation and simulation

The mechanism study was taken by DFT calculation, aiming to explore the reaction path of the H_2 release of CH_3OH driven by LBL. The ab initio MD simulations were taken to explore the decomposition of CH_3OH. The reaction rate and half-life are calculated on the basis of Eyring's transition state theory. The details of all the calculation processes and equations are available in the Supplementary Materials.

Acknowledgments

Funding: The National Natural Science Foundation of China (51832011) and the State Key Laboratory of Optoelectronic Materials and Technologies supported this work. **Author contributions:** W.C. and B.Y.: experimental work. Y.L.: calculation and simulation. Z.Z. and P.L.: data analysis. Z.K.: theoretical work. G.Y.: project planning. **Competing interests:** The authors declare that they have no competing financial interests.

Data Availability

The data that support the findings of this study are available within the article and the Supplementary Materials. Raw data are available from the corresponding authors on reasonable request.

Supplementary Materials

Calculation section
Supplementary figures
Fig. S1. The yield rate of CH_4, C_2H_4, C_2H_6, and C_2H_2 at different times under 700 mJ per pulse of laser energy.
Fig. S2. GC chromatogram of H_2 and CO released from laser-induced CH_3OH.
Fig. S3. Gibbs free energy of the formation of ions and radicals in LBL-promoted conversion of CH_3OH.
Fig. S4. Mechanism for the formation of C_2H_6, C_2H_4, C_2H_2, and CH_4 in CH_3OH decomposition reaction under pulsed laser.
Fig. S5. Carbon–carbon radial distribution functions.
Fig. S6. Each step equations of CH_3OH decomposition under pulsed laser.
Fig. S7. Mechanism and free energy profiles for CO and H_2 conversion reaction.
Fig. S8. Half-life along with reaction temperature for the formation of CHOH step in CO and H_2 conversion reaction.
Fig. S9. Hydrogen–hydrogen radial distribution functions of the cooling stage.
Fig. S10. Carbon–oxygen radial distribution functions of the cooling stage.
Fig. S11. Carbon–carbon radial distribution functions of the cooling stage.
Fig. S12. Key structures for CH_3OH decomposition under pulsed laser.

References

1. Takata T, Jiang J, Sakata Y, Nakabayashi M, Shibata N, Nandal V, Seki K, Hisatomi T, Domen K. Photocatalytic water splitting with a quantum efficiency of almost unity. *Nature*. 2020;581(7809):411–414.
2. Chen Y, Ji S, Sun W, Lei Y, Wang Q, Li A, Chen W, Zhou G, Zhang Z, Wang Y, et al. Engineering the atomic interface with single platinum atoms for enhanced photocatalytic hydrogen production. *Angew Chem Int Ed*. 2020;59(3):1295–1301.
3. Cortright RD, Davda RR, Dumesic JA. Hydrogen from catalytic reforming of biomass-derived hydrocarbons in liquid water. *Nature*. 2002;418(6901):964–967.
4. He T, Pachfule P, Wu H, Xu Q, Chen P. Hydrogen carriers. *Nat Rev Mater*. 2016;1(12):Article 16059.
5. Cohen RL, Wernick JH. Hydrogen storage materials: Properties and possibilities. *Science*. 1981;214(4525):1081–1087.
6. Olah GA. Beyond oil and gas: The methanol economy. *Angew Chem Int Ed*. 2005;44(18):2636–2639.
7. Olah GA, Prakash GKS, Goeppert A. Anthropogenic chemical carbon cycle for a sustainable future. *J Am Chem Soc*. 2011;133(33):12881–12898.
8. Palo DR, Dagle RA, Holladay JD. Methanol steam reforming for hydrogen production. *Chem Rev*. 2007;107(10):3992–4021.
9. Shao Z, Zhang S, Liu X, Luo H, Huang C, Zhou H, Wu Z, Li J, Wang H, Sun Y. Maximizing the synergistic effect between Pt^0 and $Pt^{\delta+}$ in a confined Pt-based catalyst for durable hydrogen production. *Appl Catal B Environ*. 2022;316:Article 121669.
10. Iulianelli A, Ribeirinha P, Mendes A, Basile A. Methanol steam reforming for hydrogen generation via conventional and membrane reactors: A review. *Renew Sustain Energy Rev*. 2014;29:355–368.
11. Garcia G, Arriola E, Chen W-H, De Luna MD. A comprehensive review of hydrogen production from methanol thermochemical conversion for sustainability. *Energy*. 2021;217:Article 119384.
12. Li Y, Bai X, Yuan D, Zhang F, Li B, San X, Liang B, Wang S, Luo J, Fu G. General heterostructure strategy of photothermal materials for scalable solar-heating hydrogen production without the consumption of artificial energy. *Nat Commun*. 2022;13(1):776.
13. Luo S, Lin H, Wang Q, Ren X, Hernandez-Pinilla D, Nagao T, Xie Y, Yang G, Li S, Song H, et al. Triggering water and methanol activation for solar-driven H_2 production: Interplay of dual active sites over plasmonic ZnCu alloy. *J Am Chem Soc*. 2021;143(31):12145–12153.
14. Huang J, Li G, Zhou Z, Jiang Y, Hu Q, Xue C, Guo W. Efficient photocatalytic hydrogen production over Rh and Nb codoped TiO_2 nanorods. *Chem Eng J*. 2018;337:282–289.
15. Núñez J, Fresno F, Collado L, Jana P, Coronado JM, Serrano DP, de la Peña O'Shea VA. Photocatalytic H_2 production from aqueous methanol solutions using metal-co-catalysed Zn_2SnO_4 nanostructures. *Appl Catal B: Environ*. 2016;191:106–115.
16. Pang Y, Uddin MN, Chen W, Javaid S, Barker E, Li Y, Suvorova A, Saunders M, Yin Z, Jia G. Colloidal single-layer photocatalysts for methanol-storable solar H_2 fuel. *Adv Mater*. 2019;31(49):Article 1905540.
17. Peppley BA, Amphlett JC, Kearns LM, Mann RF. Methanol-steam reforming on $Cu/ZnO/Al_2O_3$. Part 1: The reaction network. *Appl Catal A Gen*. 1999;179(1-2):21–29.
18. Sun Z, Fang S, Lin Y, Hu YH. Photo-assisted methanol steam reforming on solid solution of Cu-Zn-Ti oxide. *Chem Eng J*. 2019;375:Article 121909.
19. Rodriguez-Lugo RE, Trincado M, Vogt M, Tewes F, Santiso-Quinones G, Grutzmacher H. A homogeneous transition metal complex for clean hydrogen production from methanol-water mixtures. *Nat Chem*. 2013;5(4):342–347.
20. Irfan RM, Wang T, Jiang D, Yue Q, Zhang L, Cao H, Pan Y, Du P. Homogeneous molecular iron catalysts for direct photocatalytic conversion of formic acid to syngas ($CO+H_2$). *Angew Chem Int Ed*. 2020;59(35):14818–14824.
21. Baghdassarian O, Chu HC, Tabbert B, Williams GA. Spectrum of luminescence from laser-created bubbles in water. *Phys Rev Lett*. 2001;86(21):4934–4937.
22. Zhong X, Eshraghi J, Vlachos P, Dabiri S, Ardekani AM. A model for a laser-induced cavitation bubble. *Int J Multiph Flow*. 2020;132:Article 103433.
23. Yang GW. Laser ablation in liquids: Applications in the synthesis of nanocrystals. *Prog Mater Sci*. 2007;52(4):648–698.
24. Xiao J, Liu P, Wang CX, Yang GW. External field-assisted laser ablation in liquid: An efficient strategy for nanocrystal synthesis and nanostructure assembly. *Prog Mater Sci*. 2017;87:140–220.
25. Cui G, Yang X, Zhang Y, Fan Y, Chen P, Cui H, Liu Y, Shi X, Shang Q, Tang B. Round-the-clock photocatalytic hydrogen production with high efficiency by a long-afterglow material. *Angew Chem Int Ed*. 2019;58(5):1340–1344.